The FASEB Journal article fj.11-183145. Published online June 13, 2011.

Trpv5/6 is vital for epithelial calcium uptake and bone formation

Jo Vanoevelen,*,[1] Annelies Janssens,[†] Leonie F. A. Huitema,* Christina L. Hammond,* Juriaan R. Metz,[‡] Gert Flik,[‡] Thomas Voets,[†] and Stefan Schulte-Merker*,[§]

*Hubrecht Institute, Royal Netherlands Academy of Arts and Sciences and University Medical Centre, Utrecht, The Netherlands; [†]Laboratory for Ion Channel Research, Department of Molecular Cell Biology, Catholic University Leuven, Leuven, Belgium; [‡]Institute for Water and Wetland Research, Department of Animal Physiology, Radboud University, Nijmegen, The Netherlands; and [§]Experimental Zoology Group, Wageningen University, Wageningen, The Netherlands

ABSTRACT **Calcium is an essential ion serving a multitude of physiological roles. Aside from its role as a second messenger, it is an essential component of the vertebrate bone matrix. Efficient uptake and storage of calcium are therefore indispensable for all vertebrates. Transient receptor potential family, vanilloid type (TRPV)5 and TRPV6 channels are known players in transcellular calcium uptake, but the exact contribution of this pathway is unclear. We used forward genetic screening in zebrafish (*Danio rerio*) to identify genes essential in bone formation and identified a lethal zebrafish mutant (*matt-und-schlapp*) with severe defects in bone formation, including lack of ossification of the vertebral column and craniofacial structures. Mutant embryos show a 68% reduction in calcium content, and systemic calcium homeostasis is disturbed when compared with siblings. The phenotype can be partially rescued by increasing ambient calcium levels to 25 mM. We identified the mutation as a loss-of-function mutation in the single orthologue of TRPV5 and 6, *trpv5/6*. Expression in HEK293 cells showed that Trpv5/6 is a calcium-selective channel capable of inward calcium transport at physiological concentrations whereas the mutant channel is not. Taken together, this study provides both genetic and functional evidence that transcellular epithelial calcium uptake is vital to sustain life and enable bone formation.—Vanoevelen, J., Janssens, A., Huitema, L. F. A., Hammond, C. L., Metz, J. R., Flik, G., Voets, T., Schulte-Merker, S. Trpv5/6 is vital for epithelial calcium uptake and bone formation. *FASEB J.* 25, 000–000 (2011). www.fasebj.org**

Key Words: zebrafish · osteogenesis

Calcium (Ca^{2+}) is an essential ion that serves many physiological roles, both extra- and intracellularly. Carefully controlled intracellular Ca^{2+} concentrations are therefore indispensable to fulfill a range of biological functions, including muscle contraction, synaptic transmission, cell death, and many more (1, 2). In vertebrates, bone serves as an important Ca^{2+} store for systemic homeostasis, and plasma Ca^{2+} is in equilibrium with Ca^{2+}-hydroxyapatites in the bone matrix (3). Since such a wide variety of processes depend on the availability of Ca^{2+}, it is crucial that sufficient amounts of Ca^{2+} are taken up and the Ca^{2+} levels in body fluids are kept within a narrow concentration range (2–3 mM; ref. 4).

Terrestrial vertebrates acquire sufficient Ca^{2+} from ingested food, and the intestine therefore is the main site of uptake. There exist 2 Ca^{2+} uptake pathways: an energy-dependent transcellular pathway and a passive paracellular pathway (5). In the transcellular pathway, Ca^{2+} enters the enterocytes through the apical membrane *via* a Ca^{2+}-permeable channel of the transient receptor potential family, vanilloid type (TRPV)6 (6). In the cytosol of the enterocyte, Ca^{2+} ions are readily complexed to Ca^{2+}-buffering proteins like calbindin-D_{9K} (7). At the basal side of the epithelium, Ca^{2+} is actively extruded *via* plasma membrane Ca^{2+}-ATPase 1 (PMCA1; ref. 8) and Na^+/Ca^{2+} exchanger 1 (NCX1; ref. 9) and thus enters the blood and can be transported throughout the body. In addition, there exists a renal reabsorption pathway in which Ca^{2+} is taken up from the forming urine. Initial uptake in the kidney tubules occurs *via* TRPV5 (10), and basolateral transport is also achieved through NCX1 and PMCA1 (11). The paracellular route involves passive diffusion and mainly depends on Ca^{2+} concentration gradients and the tightness of the epithelium (12, 13). The molecular principles for transepithelial Ca^{2+} transport are highly conserved between fish and mammals (14), although their habitat is different; ambient water provides a sufficient source of Ca^{2+} (seawater: 10 mM; freshwater: 0.025–3.0 mM). In fish, Ca^{2+} is taken up mainly (~97%) by the gills, and chloride cells have long been recognized as the main cell type involved in this process

[1] Correspondence: Laboratory for Cellular Transport Systems, Department of Molecular Cell Biology, Catholic University Leuven, Herestraat 49, 3000 Leuven, Belgium. E-mail: jo.vanoevelen@med.kuleuven.be

doi: 10.1096/fj.11-183145

This article includes supplemental data. Please visit *http://www.fasebj.org* to obtain this information.

(4, 15). These cells contain all molecular components (Trpv5/6, Pmcas, and Nxc-homologues) that are thought to play a role in transepithelial Ca^{2+} uptake (16), although their contribution has never been studied at the molecular level.

The transient receptor potential (TRP) family is a large protein family consisting of several subfamilies, of which the TRPV is an example. The TRPV family can be divided into 4 groups: TRPV1/2, TRPV3, TRPV4, and TRPV5/6 (reviewed in ref. 17). TRPV1–TRPV4 are nonselective cation channels that can be activated by a number of different stimuli, such as second-messenger binding, heat and cold, and chemical and/or mechanical stress (18, 19). These channels are modestly permeable for Ca^{2+}, whereas the other 2 members of the family, TRPV5 and TRPV6, are highly selective for Ca^{2+} and tightly regulated by intracellular Ca^{2+} concentration (20–22).

An important question remaining in the field of epithelial Ca^{2+} transport concerns the exact contribution of the transcellular *vs.* the paracellular pathway (23, 24). Mouse single-knockout models for components of the transcellular pathway, Trpv5 and Trpv6, failed to answer this question due to functional redundancy and compensatory mechanisms by other genes and pathways regulating Ca^{2+} homeostasis, including parathyroid hormone- and vitamin D-dependent mechanisms (25, 26).

The vertebrate body contains a large pool of immobilized Ca^{2+} in the skeleton. Besides its role in Ca^{2+} storage, bones are important in supporting the vertebrate body, enabling movement by providing a matrix for the attachment of muscles and tendons and protection of important organs like the brain and heart (27). Skeletal homeostasis is established by balancing bone formation through the activity of osteoblasts and through bone resorption by osteoclasts, processes that exhibit a large extent of evolutionary conservation between fish and mammals (28). We used forward genetic screening in zebrafish to identify genes critically involved in bone formation and identified the single orthologue of mammalian TRPV5/6 as a main regulator of bone formation and transepithelial Ca^{2+} uptake, establishing an *in vivo* model for this essential physiological process.

MATERIALS AND METHODS

Screening procedure

Forward genetic screening was performed as described by Spoorendonk *et al.* (29).

Molecular biology

The cDNA encoding *trpv5/6* was amplified from reverse-transcribed RNA and ligated into a pGEM-T easy (Promega, Madison, WI, USA) cloning vector. For expression in HEK293 cells, the ends of the cDNA were modified with appropriate restriction sites using PCR and ligated into the pCINeo/IRES-GFP vector.

Meiotic mapping

The *matt-und-schlapp* mutation was mapped to linkage group 16 using standard simple sequence length polymorphism (SSLP) mapping. Fine mapping was performed using custom repeat markers and single-nucleotide polymorphisms (SNPs). Primer sequences are as follows: Rep12For 5′-TGGAGATTACTGTAGGTCAGAACA-3′, Rep12Rev 5′-CTGTGAAAATTGCCTTGCTC-3′; SNPAFor 5′-CCATCACTGGTGTTTTGGACT-3′, SNPARev 5′-TGAAGGAAAGCTGGTCATTTG-3′; and SNPBFor 5′-TTCTAGTGTGGACGGTGCAA-3′, SNPBRev 5′-CACCACGTTCTTGTAATGTCA-3′.

Skeletal staining

The protocol for bone and cartilage staining was adapted from Walker and Kimmel (30). Embryos were fixed in 3.5% formaldehyde and stored in 70% methanol at 4°C until further use. Embryos were partially dehydrated in 50% ethanol and stained with 0.2 mg/ml Alcian blue 8 GX (Sigma, St. Louis, MO, USA) in 70% ethanol containing 80 mM $MgCl_2$. Next, embryos were bleached in 1% H_2O_2/1% KOH for 30 min, washed in a saturated sodium tetraborate solution, and digested for 1 h in 1 mg/ml trypsin (Sigma) in 60% sodiumtetraborate. Bone was stained with 0.04 mg/ml Alizarin red S (Sigma) in 1% KOH. Finally, specimens were dehydrated to 70% glycerol and stored at 4°C.

In situ hybridization

In situ hybridization was performed essentially as described previously (31, 32). Briefly, embryos were fixed in 4% paraformaldehyde in PBS, transferred to methanol, and rehydrated. Embryos were permeablilzed by proteinase-K treatment in PBS + 0.1% Tween 20 (PBST). Embryos were prehybridized for 2 h at 68°C before overnight hybridization at 68°C in hybridization solution (50% formamide 5× SSC, 500 mg/ml yeast tRNA, 50 mg/ml heparin, 0.2% Tween 20, and 9.2 mM citric acid) containing digoxygenin-labeled antisense probes. Embryos were then washed in 2× SSCT (300 mM NaCl, 15 mM sodium citrate, and 0.1% Tween 20) and taken to 0.2 SSCT at 68°C. After graded changes to PBS, embryos were blocked for 2 h with Roche blocking reagent (Roche, Indianapolis, IN, USA) in PBS at 4°C and subsequently incubated overnight with blocking reagent containing antidioxygenin antibodies labeled with alkaline phosphatase (Roche), diluted in blocking buffer. After being washed 6 times in PBST, embryos were transferred to alkaline phosphate buffer (100 mM Tris, 50 mM $MgCl_2$, 100 mM NaCl, and 0.1% Tween 20), and staining was developed using nitroblue tetrazolium/5-bromo-4-chloro-3-indolyl phosphate. Primer sequences used to generate *in situ* probes were as follows: *trpv5/6*-5′probeFor 5′-GGGATGGAATGAAATGTTGG-3′, *trpv5/6*-5′probeRev 5′-GTGTTCATCGACCCTGGAGT-3′; *Stc-1*.2For 5′-GCAAACATCTCCTGCTTTGG-3′, *Stc-1*.2Rev 5′-TCGATATCCTGCACACTTGC-3′; *Ron2*For 5′-GTCTTCCGCATTGGACACTT-3′, *Ron2*Rev 5′-GCCGAGTCTTGTCTGAAAGG-3′; *col1a2*-5′ProbeFor 5′-AAGGACTGCAAGGACATGCT-3′, *col1a2*-5′ProbeRev 5′-TGCTCTCCAGTTGACCCTCT-3′; *col10a1*-5′ProbeFor 5′-TGCCCATGGTGAGAGATATG-3′, *col10a1*-5′ProbeRev 5′-GCATACCAGGAGCACCATTC-3′; and *spard*ProbeFor 5′-TGAGGGTTTGGATCTTCTTCC-3′, *spard*ProbeRev 5′-TGTCGACATCCTGCTCTTTG-3′. *In situ* hybridizations were performed at least 2 times, and embryos were genotyped afterward.

Genotyping

Genomic DNA of single embryos was extracted and subjected to KASPar SNP genotyping (KBiosciences, Hoddesdon, UK) using protocols described by the manufacturer. Primer sequences are as follows: ForwardSib 5′-GAAGGTGACCAAGTTC-ATGCTGTGATTTGTTTGTCTCAGGCCAGAA-3′, ForwardMut 5′-GAAGGTCGGAGTCAACGGATTGTGATTTGTTTGTCT-CAGGCCAGAT-3′, and CommonReverse 5′-GATGAGCT-GTCGGACTGGAGTCAA-3′.

Ca^{2+} and phosphorous measurements

Mutant and sibling embryos were phenotyped and overanesthetized using MS-222, washed twice with deionized water, and dried overnight under vacuum. Ions were released with 60% nitric acid. Next, samples were diluted using deionized water and measured using atomic absorption spectrophotometry (Solaar; Thermo Elemental, Winsford, UK; ref. 33). Statistical significance was determined using Student's *t* test.

Microscopy

In situ hybridizations were analyzed on a Zeiss Axioplan microscope (Carl Zeiss, Göttingen, Germany) equipped with a Leica 480C camera (Leica, Wetzlar, Germany). For analyses in transgenic backgrounds, embryos were stained *in vivo* for bone with 0.05% Alizarin red, washed with E3 medium, anesthetized with MS-222, and embedded in 0.5% agarose. Images were captured on a Leica TCS-SPE confocal microscope. Intracellular Ca^{2+}-imaging was performed using a Cell^{M} system (Olympus, Hamburg, Germany).

Transgenic lines

The *osx:nuGFP* line was generated as follows: the 4.1-kb upstream regulatory region of the medaka *osterix* gene was amplified (34) and cloned in front of a nuclear localization signal followed by GFP (nuGFP). Transgenic zebrafish were generated using the Tol2 transposon system (35). An *osc:GFP* reporter line was generated by amplification of a 3.5-kb upstream regulatory region of the medaka *osteocalcin* gene and cloned in front of GFP (36).

Evaluation of heart rates

Embryos of 54 hours postfertilization (hpf) were anesthetized using MS-222 and transferred to 24-well plates and left to acclimatize for 30 min. Heart rates were counted over intervals of 20 s, and each embryo was evaluated 3 times before genotyping.

Cell culture and transfections

HEK-293 cells were grown in DMEM medium containing 10% (v/v) fetal calf serum, 2 mM L-glutamine, 2 U/ml penicillin, and 2 mg/ml streptomycin at 37°C in an incubator with 10% CO_2. They were transfected with the pCINeo/IRES-GFP/*trpv5/6* vector using TransIT-293 transfection reagent (Mirus, Madison, WI, USA), and electrophysiological recordings were performed 24 h later.

Intracellular Ca^{2+}-imaging

Transfected cells were incubated with 2 μM fura-2 acetoxymethyl ester for 30 min at 37°C. Intracellular Ca^{2+} concentration was monitored *via* the ratio of fluorescence measured on alternating illumination at 354 and 380 nm using an MT-10 illumination system and Cell^{M} software (Olympus).

Electrophysiology

Transfected cells were identified by their green fluorescence. Patch-clamp experiments were performed in the tight-seal whole-cell configuration using an EPC-9 patch-clamp amplifier and Pulse software (HEKA Electronics, Lambrecht, Germany). Patch pipettes had DC resistances of 2–4 MΩ when filled with intracellular solution (150 mM NaCl, 5 mM $MgCl_2$, 5 mM EGTA, and 10 mM HEPES, pH 7.4). Series resistances were between 3 and 10 MΩ and were compensated 60–80%. Currents were sampled at 10 kHz and filtered at 2.9 kHz using an 8-pole Bessel filter. The stimulation protocol consisted of a linear voltage ramp from −50 to +100 mV (in 400 ms), which was applied every 5 s. The divalent cation-free extracellular solutions contained 150 mM XCl [where X = Na^+, K^+, or *N*-methyl-D-glucamine (NMDG)] and 10 mM HEPES, titrated to pH 7.4 with XOH. Isotonic divalent cation solutions contained 100 mM XCl_2 (where X = Ca, Ba, or Mg) and 10 mM HEPES, titrated to pH 7.4 with $X(OH)_2$. For the anomalous mole fraction behavior, NaCl and $CaCl_2$ solutions were mixed. All experiments were performed at room temperature (20–22°C).

Ca^{2+} enrichment and depletion

Embryos were collected and transferred to modified E3 medium (5 mM NaCl, 0.17 mM KCl, and 0.33 mM $MgSO_4$; ref. 37) supplemented with the indicated amounts of total Ca^{2+} and incubated at 28,5°C. Embryos were fixed at 7 days postfertilization (dpf) and processed for cartilage and bone staining.

RESULTS

Matt-und-schlapp phenotype

Matt-und-schlapp (German for "slack as a rag") embryos completely lack ossification of the axial skeleton (**Fig. 1*A***). They fail to inflate their swim bladder and die at 7–9 dpf. Analysis of the phenotype at 7 dpf revealed some phenotypic variability in terms of ossification (Fig. 1*A*). Mutants were scored as mild when they lacked ossification of the axial skeleton but possessed some normally ossified craniofacial elements such as cleithrum, opercle, parasphenoid, and the teeth on the fifth branchial arch. Mineralization of the teeth was reduced in the mild phenotype. Mutants were categorized as severe when all ossification was absent, except for the otoliths. Bright field images (Fig. 1*A*, insets) of the mutant embryos illustrate that the tip of the notochord is formed correctly, but ossification is absent. Otoliths (which are mineralized, nonbone structures) are present but remain smaller in size. All cartilage elements are present and indistinguishable between siblings and mutants.

Matt-und-schlapp encodes trpv5/6

Genome scan analysis linked the mutation to linkage group (LG) 16 (Fig. 1*B*). With the use of standard

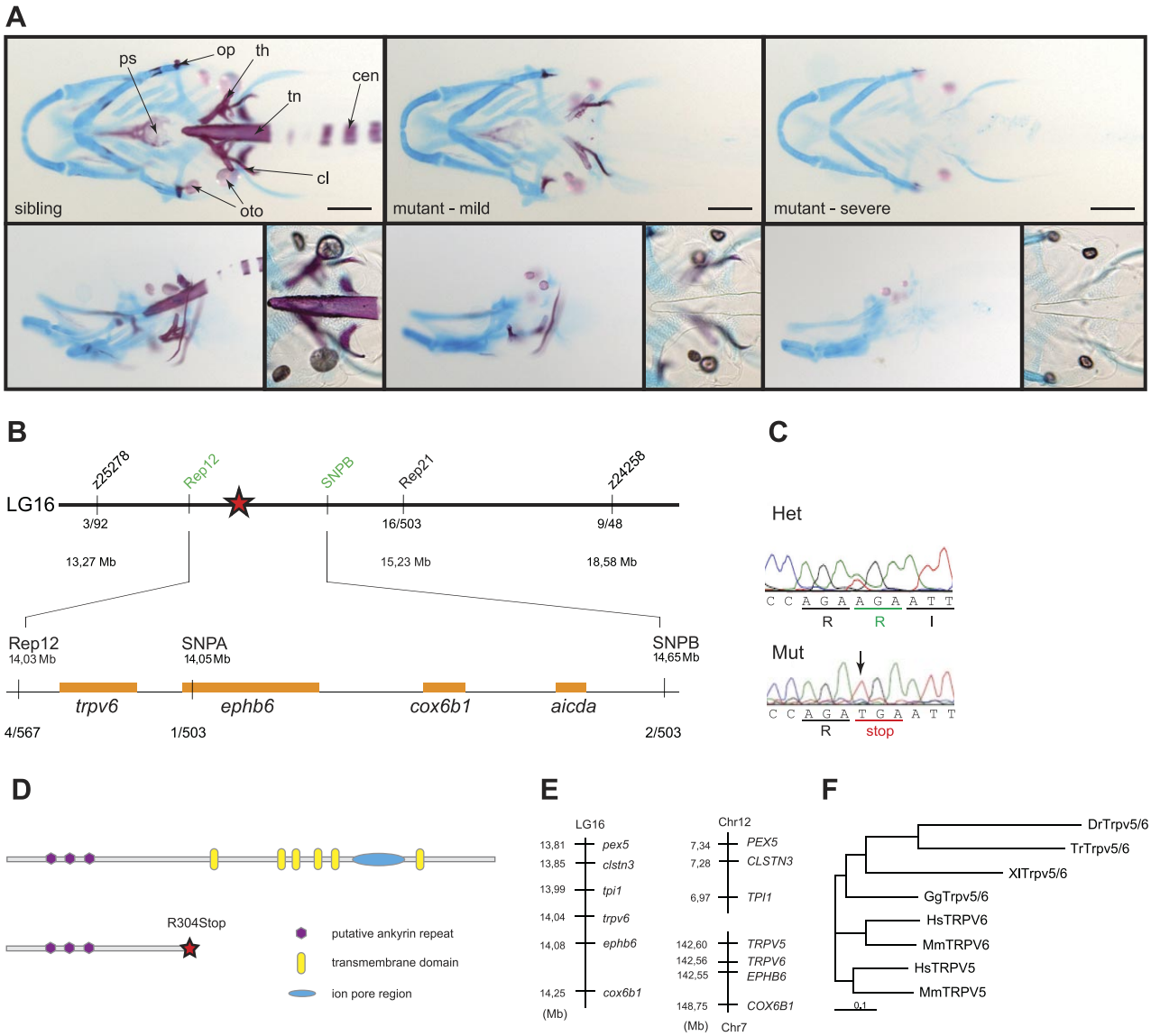

Figure 1. Phenotypic description and mapping of *mus*. *A*) Bone (red) and cartilage (blue) staining of sibling and mutant embryos at 7 dpf. Top panels: ventral view of sibling, mild mutant, and severe mutant phenotypes, respectively. Bottom left and middle panels: embryos in side view. Bottom right panels: detail of the tip of the notochord. Key skeletal elements are indicated: ps, parasphenoid; op, opercle; th, teeth; oto, otoliths; tn, tip of the notochord; cl, cleithrum; cen, vertebral centrum. Scale bars = 100 μm. *B*) Overview of meiotic mapping strategy. Numbers indicate number of recombinants/number of mutant embryos and the genomic location (in Mb) according to the Ensemble zebrafish genome browser (Zv9). Markers Rep12 and Rep21 are flanking markers restricting the critical region to ~2 Mb. This region was narrowed further by single-embryo mapping using SNP markers. Markers Rep12 and SNPA demarcate a region of interest containing only 1 gene: *trpv5/6*. *C*) Sequencing of mutant and heterozygous cDNA. Causative mutation is identified as an A to T substitution resulting in an amino acid change of arginine (R) to a premature stop codon (R304Stop). *D*) Top: schematic depiction of the wild-type Trpv5/6 protein with putative functional domains indicated. Bottom position of the mutation resulting in a premature stop codon. *E*) Synteny of chromosome regions at the position of *trpv5/6* between zebrafish and human chromosomes. Numbers (Mb) represent the chromosomal positions of the respective genes. The order of a number of genes in the region is conserved between zebrafish LG16 and parts of human chromosome 7 and 12. Note the absence of a second isoform of *trpv5/6* in zebrafish. *F*) Phylogenetic analysis of TRPV5/6 genes in mammals: *Homo sapiens* (Hs) and *Mus musculus* (Mm); birds: *Gallus gallus* (Gg); amphibians: *Xenopus laevis* (Xl); and fish: *Takifugu rubripes* (Tr) and *Danio rerio* (Dr). Only mammals show 2 distinct TRPV5/6-genes; amphibians and fish genomes only contain 1 *trpv5/6* gene. Phylogenetic tree (guide tree) was constructed using the neighbor-joining method in Vector NTI (Invitrogen) and visualized using TreeView software.

SSLP mapping, the region of interest was reduced to 1 Mb using custom repeat markers. Finally, by identification of informative SNPs, the region was further reduced to an interval of 50 kb containing a single gene: *trpv5/6*, a member of the TRPV family (Fig. 1*B*). Sequencing of the *trpv*5/6-encoding cDNA in siblings and mutants revealed a single A to T nucleotide change resulting in a premature stop codon at position 304 (R304Stop) of the predicted protein (Fig. 1*C*).

Characterization of *trpv5/6*

The *trpv5/6* gene is composed of 18 exons spanning 31 kb on LG16. The mutation *mus*^{t25927} is located in exon 9. The resulting wild-type protein consists of 709 aa with a predicted molecular mass of 81.1 kDa (Fig. 1*D*). The mutated protein R304Stop results in a severely truncated protein containing only 303 of the predicted 709 aa and is lacking all putative transmembrane domains including the pore region (Fig. 1*D*). Mammalian genomes contain 2 genes coding for epithelial calcium channels (ECaCs), which were initially termed *ECaC1* (or *CaT2*; ref. 10) and *ECaC2* (*CaT1*; ref. 6) and later renamed *TRPV5* and *TRPV6*, respectively. The zebrafish, amphibian, and avian genomes contain only one ECaC isoform (*trpv5/6*; Fig. 1*E*, *F*). Figure 1*E* shows a large degree of synteny in the region of trpv5/6 on LG16 of the zebrafish genome and chromosomes 12 and 7 of the human genome and illustrates the juxtaposed location of *TRPV5* and *TRPV6* in the human genome. No second homologue could be detected in zebrafish. Phylogenetic analysis further shows that mammalian TRPV5 and TRPV6 do not cluster together in the same groups, nor do the nonmammlian isoforms. This notion and the adjacent position of *TRPV5* and *TRPV6* on the same chromosome in mammals support the notion of a gene duplication event in mammals that occurred after the divergence of mammalian and other vertebrate *Trpv5/6*, which is in line with other phylogenetic studies comparing mammalian isoforms to other vertebrate species (38).

Trpv5/6 mRNA expression was first observed at 24 hpf in the epithelial layer covering the yolk sac and yolk extension (**Fig. 2*C***). At later stages (4 dpf), expression was still present in the skin, but highest expression levels were in the branchial region where the gills will form (Fig. 2*B*). In mutant embryos, *trpv5/6* expression was absent at 24 hpf (Fig. 2*B*) and severely reduced at later stages (4 dpf) when compared with siblings (Fig. 2*C*). Under standard rearing conditions (0.33 mM total Ca^{2+} in the E3 embryo medium; ref. 37), ~25% of the embryos from a heterozygous parental pair showed the phenotype, as predicted for a recessive mutation (Fig. 2*A*).

Mutants have very low Ca^{2+} content and can be rescued by extracellular Ca^{2+}

Since mammalian TRPV5 and TRPV6 are Ca^{2+}-selective channels involved in active Ca^{2+} reabsorption, we investigated the overall Ca^{2+} content in mutant *vs.* sibling embryos by atomic absorption spectrometry. Mutant embryos showed a reduction in Ca^{2+} content of 68% (8695 *vs.* 2732 ppb/mg protein; $P<0.05$) when compared with siblings (**Fig. 3*A***). We also measured the phosphorous content of the same samples (Fig. 3*B*). Here, the difference was much smaller and not statistically significant (18%; 13,620 *vs.* 11,204 ppb/mg protein) but in line with the observed reduction of mineralized bone in the mutant embryos (Fig. 1*A*). To further test whether the mutants displayed systemic Ca^{2+} deficiency, we investigated the expression of stanniocalcin 1 (*stc1*), an antihypercalcaemic hormone secreted by the corpuscles of Stannius (39, 40), fish-specific endocrine organs involved in Ca^{2+} metabolism (40, 41). *Stc1* expression was completely absent in mutant embryos (Fig. 3*C*) even though the corpuscules of Stannius were correctly formed, as indicated by *ron2* expression. *Ron2* is a tyrosine-receptor kinase expressed in the corpuscules of Stannius and pronephric ducts (Fig. 3*D*). As the reduced whole-body Ca^{2+} content was suggestive of a defect in Ca^{2+} uptake, we exposed mutant embryos to different concentrations of extracellular Ca^{2+}, ranging from a minimal (nominally 10 μM total Ca^{2+}) or a standard amount (0.33 mM total Ca^{2+}) to a very high amount (25 mM total Ca^{2+}; Fig. 2*A*). Under conditions of low-Ca^{2+} availability (10 μM), a mortality rate corresponding to the predicted fraction of mutant embryos (~25%) was observed. This shows that mutant embryos are hypersensitive to low Ca^{2+} availability. Under conditions of normal Ca^{2+} (0.33 mM; the concentration used under standard

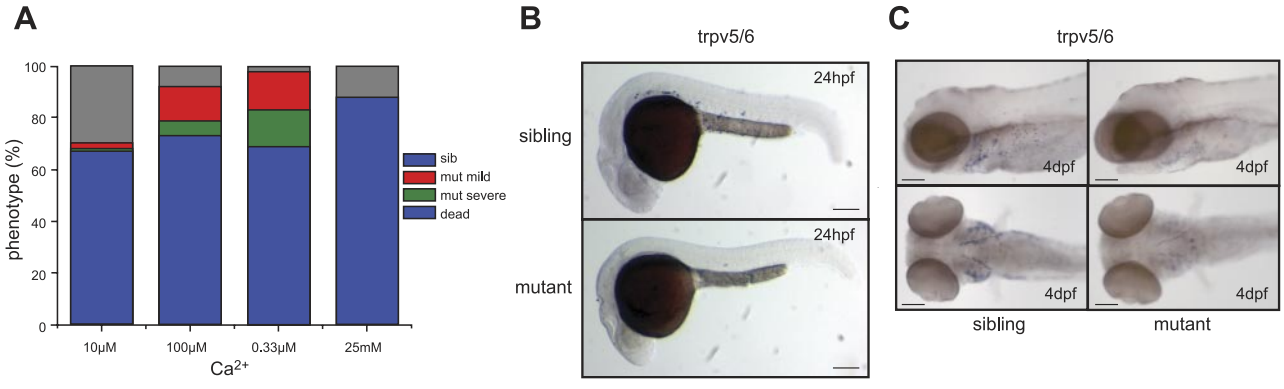

Figure 2. Phenotype dependence on Ca^{2+} and expression pattern. *A*) Distribution of the phenotypes in embryos grown in different extracellular Ca^{2+} concentrations. Same classification of mild and severe phenotypes as in Fig. 1*A* is used here. In standard growing conditions, the total extracellular Ca^{2+} concentration is 0.33 mM. Stacked bars represent the percentage of phenotypes from a total of 150 embryos/condition from 3 independent experiments. *B, C*) *trpv5/6* mRNA expression pattern in sibling and mutant embryos using *in situ* hybridization at 24 hpf (*B*) and at 4 dpf (*C*).

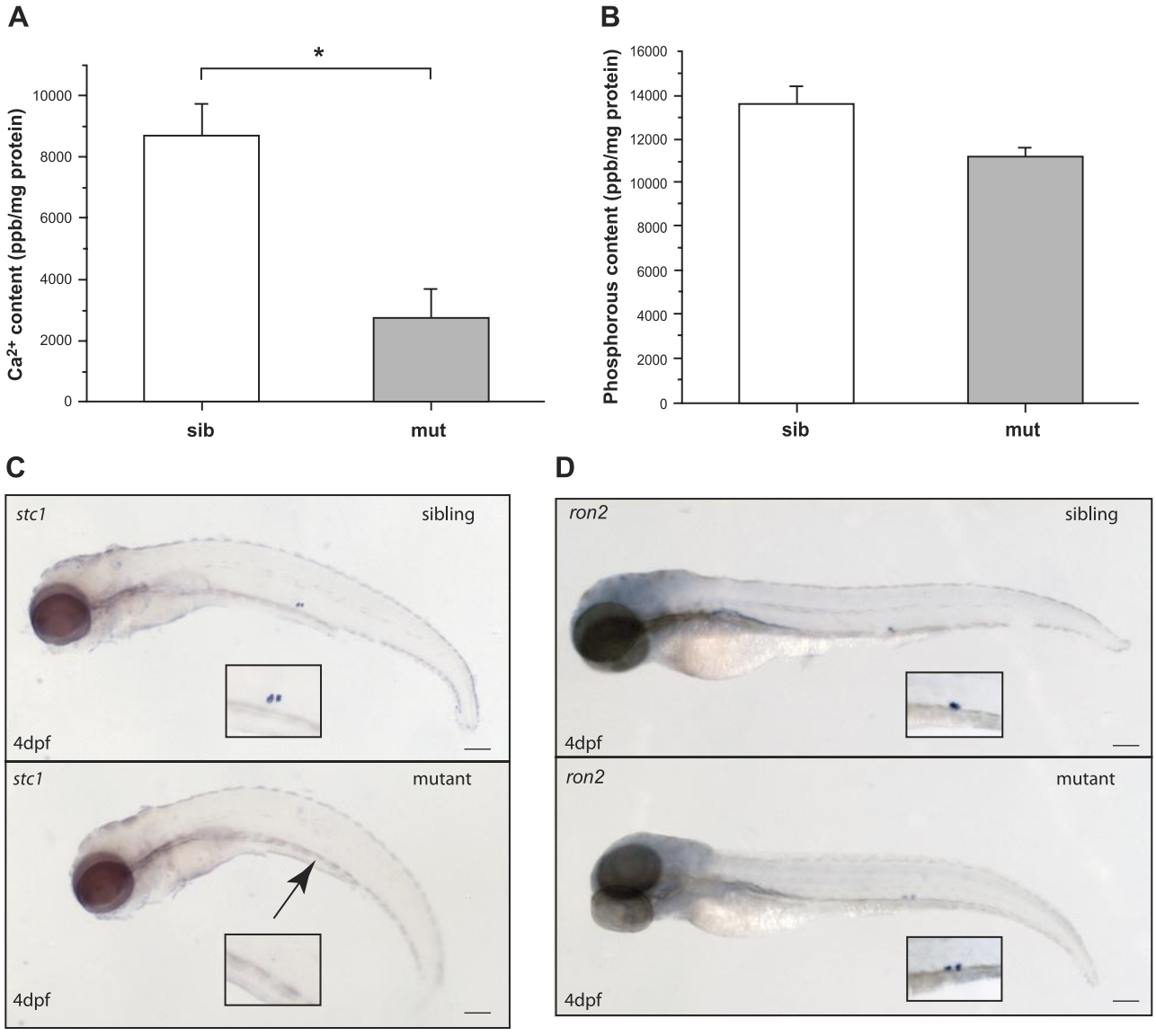

Figure 3. Ca^{2+} deficiency and disturbed Ca^{2+} homeostasis in *mus* mutants. *A*) Quantification of Ca^{2+} content in mutant and sibling embryos at 6 dpf using atomic absorption spectrometry. Mutants contain significantly ($P<0.05$) less Ca^{2+} when compared with siblings. Measurements are average values of 3 independent experiments measuring a total of 19 single embryos/condition. *B*) Determination of phosphorous content, as a measure for the amount of phosphate, at 6 dpf in sibling and mutant embryos using atomic absorption spectrometry. Phosphorous content is only modestly lower (not significant) in mutants. This difference is attributed to the presence of less bone in the mutants. Same samples as in *A* were used. *C*) Expression of *stanniocalcin 1* (*stc1*) in embryos at 4 dpf using *in situ* hybridization. Insets: detailed view of expression in the corpuscules of Stannius. Scale bars = 100 μm. *D)* Expression of r*on2* in embryos at 4 dpf. Expression of *ron2* is present in both siblings and mutants indicating that the corpuscules of Stannius are formed correctly despite lacking *stc1* expression. Scale bar = 100 μm. *E*) Heart rates in a clutch of *mus* embryos. Average heart rates were counted in 48 anesthetized embryos at 54 hpf. Each embryo was evaluated 3 times before genotyping; n = number of embryos of each genotype that were evaluated. Statistical significance was determined using a Student's t test. Values are depicted as average ± SD.

rearing conditions), the predicted fraction of mutant phenotypes (~25%) was observed with an equal distribution between mild and severe phenotypes (Fig. 2*A*). At 25 mM Ca^{2+}, no mutant phenotypes were observed (Fig. 2*A*) but lethality past 7–9 dpf could not be overcome. Taken together, these results

show that mutant embryos are hypersensitive to low-Ca^{2+} availability and can be rescued by high Ca^{2+} concentrations in the medium, indicating defects in Ca^{2+} uptake. We also tested whether other Ca^{2+}-dependent physiological processes are affected in *mus* mutants. Heart contraction was evaluated, and no difference between genotypes could be observed (Fig. 3*E*). Mutant embryos also still exhibited a touch response, indicating that skeletal muscles and the sensory system were functional. To address the question of whether the observed bone phenotypes are specifically due to nonfunctional Trpv5/6 channels or an effect secondary to Ca^{2+} deficiency, we repeated rearing wild-type embryos in different Ca^{2+} concentrations (Supplemental Fig. S1). When normal embryos were grown in low amounts (5 and 10 μM added Ca^{2+}) of extracellular Ca^{2+}, the same bone phenotypes were observed (Supplemental Fig. S1). *Stc1* expression in wild-type embryos grown in low Ca^{2+} was also severely reduced (Supplemental Fig. S1*C*). Thus, the bone phenotype of *mus* embryos can be phenocopied in wild-type embryos by severely restricting the extracellular Ca^{2+} concentration. Taken together, these data support the notion that *mus* mutant embryos suffer from Ca^{2+} deficiency, which is primarily reflected by the absence of ossification of the axial skeleton, whereas other functions that highly depend on Ca^{2+} appear normal at least until d 7.

Mineralization is impaired in *mus* mutants while differentiated osteoblasts are present

To uncover whether the lack of ossification in mutant embryos was due to general Ca^{2+} deficiency or to a lack of osteoblast differentiation, we crossed the *mus* allele into transgenic reporter lines marking early (*osx:nuGFP*; ref. 34) and mature (*osc:GFP*) osteoblasts (36) respectively. *Osterix* expression in mutant embryos was indistinguishable from that in sibling embryos and corresponded to the ossified structures, as visualized by Alizarin red staining (**Fig. 4*A***). Significantly, there was an absence of ossification of the tip of the notochord and the forming vertebrae in mutants, a hallmark of the mutant phenotype. As expected, the number of differentiated (*osc*-positive) osteoblasts was less than the amount of undifferentiated (*osx*-positive) osteoblasts, since osteoblast development is still in progress at this stage. *Osterix* espression indicates that spatially and temporally development of early osteoblasts takes place in *mus* mutants. *Osteocalcin* expression, however, was absent in *mus* mutant embryos (Fig. 4*B*). To show whether this lack of *osteocalcin* expression was due to lack of osteoblast differentiation or to dependence of *osteocalcin* expression on Ca^{2+} availability, we explored the expression of other late osteoblast markers (*col1a2*, *col10a1*) using *in situ* hybridization (Fig. 4*C*). The expression patterns of both *col1a2* and *col10a1* were indistinguishable between siblings and mutant em-

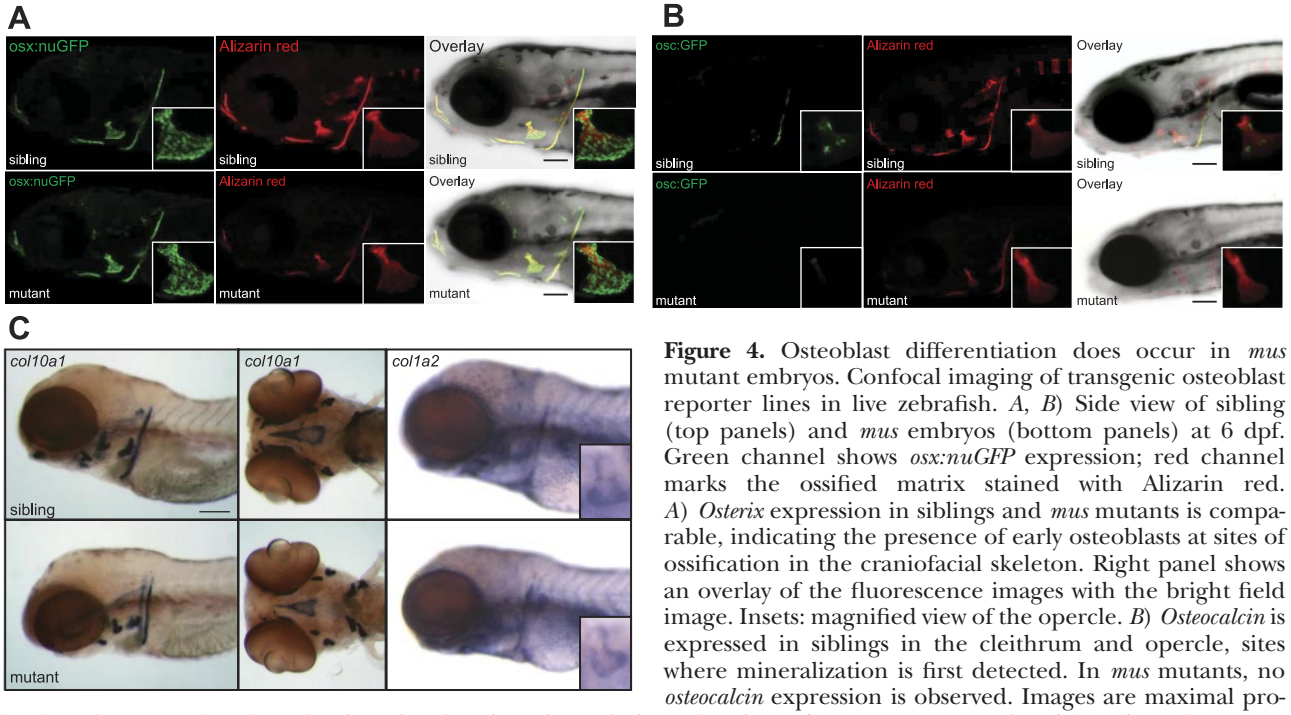

Figure 4. Osteoblast differentiation does occur in *mus* mutant embryos. Confocal imaging of transgenic osteoblast reporter lines in live zebrafish. *A*, *B*) Side view of sibling (top panels) and *mus* embryos (bottom panels) at 6 dpf. Green channel shows *osx:nuGFP* expression; red channel marks the ossified matrix stained with Alizarin red. *A*) *Osterix* expression in siblings and *mus* mutants is comparable, indicating the presence of early osteoblasts at sites of ossification in the craniofacial skeleton. Right panel shows an overlay of the fluorescence images with the bright field image. Insets: magnified view of the opercle. *B*) *Osteocalcin* is expressed in siblings in the cleithrum and opercle, sites where mineralization is first detected. In *mus* mutants, no *osteocalcin* expression is observed. Images are maximal projections from a series of confocal stacks of each embryo. At least 4 embryos/genotype were analyzed in at least 2 separate experiments. *C*) Expression of additional late osteoblast markers in sibling and *mus* embryos at 4 dpf. Two markers of differentiated osteoblasts, *col1a2* and *col10a1*, were examined using *in situ* hybridization. *Col1a2* and *col10a1* expression is shown at the cleithrum, opercle, parasphenoid, teeth on the 5th branchial arch, and lower jaw, which are the first elements to be mineralized. Insets: details of the opercle showing *col1a2* expression. No differences between sibling and *mus* embryos were detected. Expression patterns of 20–30 embryos of a single clutch were analyzed; embryos used for imaging were subsequently genotyped. Scale bars = 100 μm.

bryos; the elements that are first to mineralize showed the presence of differentiated osteoblasts: cleitrum, opercle, teeth on the fifth branchial arch, parasphenoid, and Meckel's cartilage. The expression pattern of an additional late osteoblast marker, *sparc* (*osteonectin*), also showed no difference in expression in mutant *vs.* sibling embryos (Supplemental Fig. S3). Since only the *osteocalcin* expression pattern was altered in the mutant embryos, we concluded that mature osteoblasts exist in *mus* mutant embryos and that *osteocalcin* expression is dependent on the availability of sufficient Ca^{2+}, while expression of other markers is not.

Trpv5/6 is a Ca^{2+}-selective cation channel

To investigate the characteristics of Trpv5/6, wild-type Trpv5/6 was expressed in HEK293 cells, a well-established overexpression host, and ion currents were recorded in whole-cell patch-clamp experiments. In divalent cation-free conditions with Na^+ or K^+ (150 mM) as the sole extracellular cation, we measured strongly inwardly rectifying currents that reversed around 0 mV, whereas no inward current could be measured when the large cation $NMDG^+$ was the only extracellular cation (**Fig. 5*A***). These data indicate that Trpv5/6 is an inwardly rectifying cation channel, permeable to Na^+ and K^+. In isotonic $CaCl_2$ solution (100 mM), the reversal potential shifted toward positive potentials, indicative of a Ca^{2+}-selective current (Fig. 5*B*). From the reversal potential of 56 ± 7 mV, we calculated a relative permeability (P_{Ca}/P_{Na}) of 120 ± 13. We also measured significant permeability for Ba^{2+} (P_{Ba}/P_{Na}=38±13), whereas no inward currents could be measured with Mg^{2+} as the sole charge carrier (Fig. 5*B*). Increasing extracellular Ca^{2+} from 1 μM to 100 mM revealed anomalous mole fraction behavior (Fig. 5*C*). This is a hallmark of highly Ca^{2+}-selective channels and reflects inhibition of inward Na^+ current at low Ca^{2+} concentrations and Ca^{2+} permeation at higher concentrations. Taken together, these results demonstrate that Trpv5/6 is a Ca^{2+}-selective channel, analogous to mammalian isoforms. Whereas mammalian TRPV5 and TRPV6 are similar in their biophysical properties, they differ in their sensitivity to block by ruthenium red (RR). We found that the RR sensitivity of Trpv5/6 was more comparable with that of mammalian TRPV6, with only partial inhibition at 10 μM and an IC_{50} value of 4 μM (Fig. 5*D*, *E*). To directly show whether the channel resulting from the *mus* mutation was functional, we also expressed the mutant channel and ion currents were measured. Almost no current was observed in the presence of Na^+ (Supplemental Fig. S2*A*) or Ca^{2+} (Supplemental Fig. S2*B*) in the mutant channel, whereas the wild-type channel was an inwardly rectifying, Ca^{2+}-selective channel (Supplemental Fig. S2*A*, *B*). Quantification of the amount of current at −100 mV in the presence of Na^+ or Ca^{2+} is shown in Supplemental Fig. S2*C*, *D*. These results confirm that the mutation is a loss-of-function mutation, as predicted from the position of the mutation early in the coding sequence.

We also performed cytosolic Ca^{2+} measurements to directly show inward Ca^{2+} transport from the extracellular space to the cytosol *via* Trpv5/6 (**Fig. 6**). A concentration-dependent cytosolic response of Ca^{2+} on addition of increasing amounts of extracellular Ca^{2+} was observed (Fig. 6). Note that a large cytosolic response was already observed at concentrations <0.33 mM Ca^{2+}, corresponding to the concentration used in normal E3 medium. This supports the view that Trpv5/6 is capable of epithelial Ca^{2+} uptake under physiological growth conditions.

DISCUSSION

The phenotype was termed *matt-und-schlapp*, referring to the loss of rigidity in the absence of an ossified vertebral column. The expression pattern of *trpv5/6* confirms the results of previous studies showing that expression in zebrafish commences at 24 hpf and becomes restricted to the skin and gill area (4). With the use of RT-PCR, however, expression of *trpv5/6* was shown in all tissues tested, with highest levels in gill, intestine, and kidney (4). In addition, these researchers showed that the number of *trpv5/6*-expressing cells is dependent on the extracellular Ca^{2+} concentration (4). Gill expression has also been shown for *trpv5/6* of other fish species (38). We show that levels of mRNA

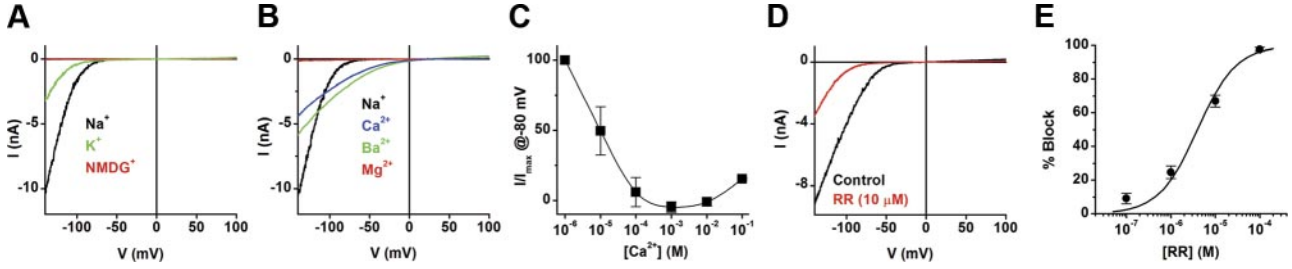

Figure 5. Trpv5/6 is a calcium-selective cation channel. Whole-cell patch-clamp experiments on Trpv5/6-overexpressing HEK293 cells. *A*) Current-voltage (*I-V*) relations when using Na^+ (black trace), K^+ (green trace), or $NMDG^+$ (red trace) as the sole cation in the extracellular solution. *B*) Comparison of current-voltage relations obtained with Na^+, Ba^{2+}, Ca^{2+}, or Mg^{2+} as the sole extracellular cation. *C*) Anomalous mole fraction behavior when extracellular Ca^{2+} is increased from 1 μM to 100 mM. *D*) Current-voltage relations showing partial block of Trpv5/6 currents in the presence of 10 μM RR. *E*) Dose-response curve for the inhibition of Trpv5/6 by RR.

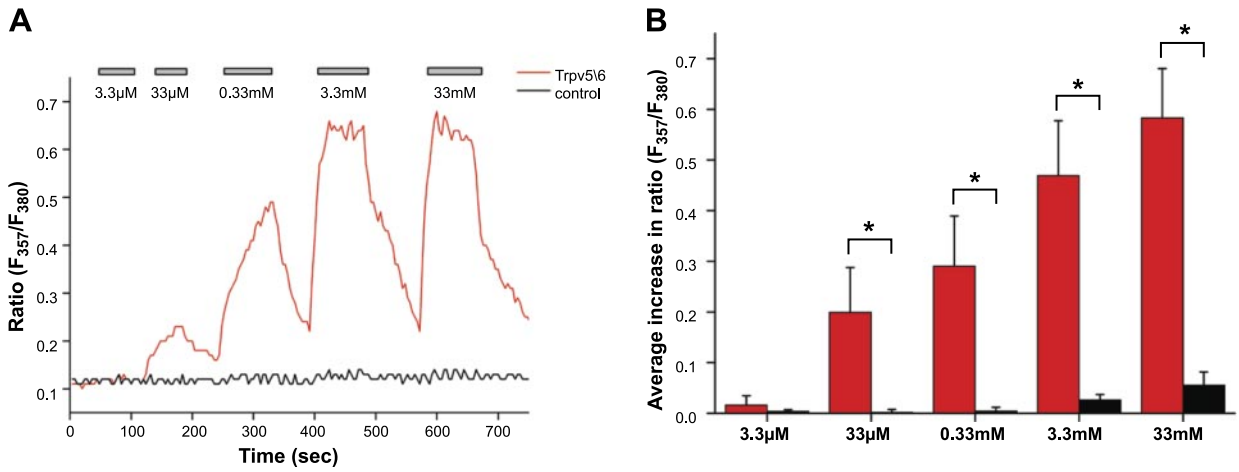

Figure 6. Direct measurement of Ca^{2+} influx. Cytosolic Ca^{2+} measurements in HEK293 cells expressing Trpv5/6 (red trace) or with no overexpression (black trace) using Fura-2. *A*) Representative experiment illustrating responses of cytosolic Ca^{2+} on addition of increasing concentrations of extracellular Ca^{2+}. *B*) Cytosolic responses of Trpv5/6-expressing cells (red bars) *vs.* control cells (black bars) were quantified. Bars represent the average cytosolic response of 33 Trpv5/6-expressing cells and 27 control cells from 7 experiments. Values are depicted as average ± SE. *$P<0.01$; Student's *t* test.

expression differ between siblings *vs.* mutants. At 24 hpf, there is no detectable *trpv5/6* expression in the mutants, while at 4 dpf, there is markedly less *trpv5/6* expression in mutant embryos, suggesting degradation of the mutant mRNA by nonsense-mediated decay (42).

The lack of *stc1* expression is not surprising, since *stc1* mRNA levels are regulated by extracellular Ca^{2+}, and, in turn, *trpv5/6* expression is down-regulated when Ca^{2+} is present in sufficient amounts (40). Incubation of embryos in low Ca^{2+}-containing medium resulted in up-regulation of *trpv5/6* and down-regulation of *stc1* (40), indicative of a tight relation among extracellular Ca^{2+}, *stc1*, and *trpv5/6* expression. *Mus* mutant embryos experience Ca^{2+} deficiency since there is no functional *trpv5/6*, which is (insufficiently) counteracted by down-regulation of the antihypercalcaemic hormone *stc1*.

The fact that the mutant phenotype is observed in the vertebral column is most likely due to developmental timing: vertebrae are formed relatively late in development. During early stages of development, there is sufficient Ca^{2+} present in the yolk (43), and embryos can take up Ca^{2+} in adequate amounts for initial growth and survival (44). These sources suffice to allow ossification in those structures that are first to ossify (3 dpf), like cleithrum and opercle. As development proceeds, there is an increasing need for Ca^{2+} (43) and *trpv5/6*-independent mechanisms are not able to supply this amount. As a result, no bone is formed in structures that ossify later in development such as the tip of the notochord and the vertebrae.

Our data show that *mus* mutants suffer from general Ca^{2+} deficiency. Arguments for this notion are as follows: significantly reduced Ca^{2+} content, loss of *stc1* expression, phenocopy in wild-type embryos by restricting Ca^{2+} availability, and hypersensitivity to low Ca^{2+} and rescue by high Ca^{2+}. This phenotype strongly suggests the existence of a hierarchy in the use of Ca^{2+}: the limited amount of Ca^{2+} that is present is used primarily to fulfill other essential cell biological functions such as muscle contraction and secretion at the expense of bone formation.

Skeletal defects have been reported in zebrafish mutants defective in other members of the TRP family. The *touchtone/nutria* allele (*trpm7*) shows growth retardation and alterations in skeletal development (45). In contrast, *trpm7* mutations and subsequent disturbance in Ca^{2+} and Mg^{2+} homeostasis were found to be associated with elevated levels of *stc1* (46). This is probably due to residual activity, since the allele is not a full loss of function. Furthermore, another TRP channel, TRPV4, has recently attracted significant attention since it was linked to human bone diseases (47, 48) and neurological disorders (49, 50).

Whereas mammalian TRPV5 and TRPV6 are very similar in their biophysical properties, they differ significantly in their sensitivity to block by RR, with IC_{50} values of 121 nM for TRPV5 compared with 9 μM for TRPV6 (51). We found that the RR sensitivity of zebrafish Trpv5/6 is more comparable to that of mammalian TRPV6, with an IC_{50} value of 4 μM. These results, combined with phylogenetic analysis in zebrafish and pufferfish (52) and the absence of a second isoform in fish, suggest that mammalian isoforms have evolved separately from the other vertebrates and the ancestral gene was duplicated after this event. The ancestral isoform probably resembled TRPV6 most and was duplicated as an adaptation to terrestrial life.

The *mus* phenotype is much more severe than the phenotypes observed for knockouts of its murine counterparts. *Trpv5*$^{-/-}$ mice display reduced renal Ca^{2+} reabsorption resulting in hypercalciuria and show only mild disturbances in bone structures (26). *Trpv5* was also described as essential for osteoclast function (53). *Trpv6*-deficient mice also show impaired Ca^{2+} homeostasis manifested as decreased intestinal Ca^{2+} absorption, poor weight gain, decreased bone mineral density, and reduced fertility (25). In addition, TRPV6 is involved in maternal-fetal Ca^{2+} transport (54). The mildness of phe-

notypes is best explained by redundancy and compensatory mechanisms: in *Trpv5*-knockout mice, loss of Ca^{2+} *via* the urine is compensated by TRPV6-mediated Ca^{2+} hyperabsorption in the intestine. On the other hand, *Trpv5* up-regulation is not shown to occur in *Trpv6*-knockout mice, although compensatory hypercalcemic PTH and vitamin-D pathways are activated (25, 55). This indicates that TRPV6 is not essential for intestinal Ca^{2+} uptake, unless Ca^{2+} availability is restricted (56, 57). A double knockout cannot be generated by crossing both strains, since *Trpv5* and *Trpv6* are located adjacent to each other on the same chromosome. Targeted inactivation of the other known components of transcellular transport, *Ncx1* and *Pmca1*, could not reveal their importance in transepithelial Ca^{2+} transport, since the respective knockout mice are not viable (58, 59). Our study shows that if the gatekeeper of the transcellular pathway is deficient, Ca^{2+} cannot be transported adequately to sustain life. The paracellular pathway or other processes cannot compensate for the loss of this essential component. Zebrafish are an attractive model for these studies since all molecular components are conserved, but they contain only 1 gatekeeper gene and have fewer compensatory mechanisms, resulting in a fully informative loss-of-function phenotype. In this study, we provide for the first time genetic and functional evidence for an essential role of Trpv5/6 in systemic Ca^{2+} uptake and bone formation. We show that in zebrafish, the transcellular uptake route for Ca^{2+} in the gills is the most important mechanism for Ca^{2+} uptake, and Trpv5/6 is a key molecular player in this process. Using electrophysiological techniques and Ca^{2+} imaging, we could demonstrate that Trpv5/6 is a highly Ca^{2+}-selective channel that allows Ca^{2+} influx under physiological conditions.

In summary, this study shows for the first time an animal model lacking active transepithelial Ca^{2+} transport, indicating the essential role of this process to sustain life and enable bone formation. We further show that Trpv5/6 is an essential molecular player in this process. The *mus* zebrafish mutant line can therefore serve as an important screening tool for regulators of transepithelial Ca^{2+} uptake, bone density, and related disorders, such as osteoporosis. FJ

The authors thank L. Lieben, G. Carmeliet and B. Nilius for helpful discussions. The authors acknowledge the Hubrecht Imaging Center for expert advice on imaging. The authors thank the Tübingen 2000 screen consortium for identifying the *mus*^{t25927} allele; this mutant was identified while S.S-M was working at Artemis Pharmaceuticals/Exelixis Deutschland. S.S.-M. is supported by the Koninklijke Nederlandse Academie van Wetenschappenand funding from SmartMix. J.V. is a Postdoctoral Fellow of the Fonds voor Wetenschappelijk Onderzoek–Vlaanderen. The authors declare no conflicts of interest. The data reported in this study have been deposited in the GenBank database (accession no. HQ676591; http://www.ncbi.nlm.gov).

REFERENCES

1. Vangheluwe, P., Sepulveda, M. R., Missiaen, L., Raeymaekers, L., Wuytack, F., and Vanoevelen, J. (2009) Intracellular Ca^{2+}- and Mn^{2+}-transport ATPases. *Chem. Rev.* **109,** 4733–4759
2. Peacock, M. (2010) Calcium metabolism in health and disease. *Clin. J. Am. Soc. Nephrol.* **5**(Suppl. 1), S23–S30
3. Witten, P. E., and Huysseune, A. (2009) A comparative view on mechanisms and functions of skeletal remodelling in teleost fish, with special emphasis on osteoclasts and their function. *Biol. Rev. Camb. Philos. Soc.* **84,** 315–346
4. Pan, T. C., Liao, B. K., Huang, C. J., Lin, L. Y., and Hwang, P. P. (2005) Epithelial Ca^{2+} channel expression and Ca^{2+} uptake in developing zebrafish. *Am. J. Physiol. Regul. Integr. Comp. Physiol.* **289,** R1202–1211
5. Hoenderop, J. G., Nilius, B., and Bindels, R. J. (2005) Calcium absorption across epithelia. *Physiol. Rev.* **85,** 373–422
6. Peng, J. B., Chen, X. Z., Berger, U. V., Vassilev, P. M., Tsukaguchi, H., Brown, E. M., and Hediger, M. A. (1999) Molecular cloning and characterization of a channel-like transporter mediating intestinal calcium absorption. *J. Biol. Chem.* **274,** 22739–22746
7. Lee, G. S., Lee, K. Y., Choi, K. C., Ryu, Y. H., Paik, S. G., Oh, G. T., and Jeung, E. B. (2007) Phenotype of a calbindin-D9k gene knockout is compensated for by the induction of other calcium transporter genes in a mouse model. *J. Bone Miner. Res.* **22,** 1968–1978
8. Hoenderop, J. G., Hartog, A., Stuiver, M., Doucet, A., Willems, P. H., and Bindels, R. J. (2000) Localization of the epithelial Ca(2+) channel in rabbit kidney and intestine. *J. Am. Soc. Nephrol.* **11,** 1171–1178
9. Kikuchi, K., Kikuchi, T., and Ghishan, F. K. (1988) Characterization of calcium transport by basolateral membrane vesicles of human small intestine. *Am. J. Physiol.* **255,** G482–489
10. Hoenderop, J. G., van der Kemp, A. W., Hartog, A., van de Graaf, S. F., van Os, C. H., Willems, P. H., and Bindels, R. J. (1999) Molecular identification of the apical Ca^{2+} channel in 1, 25-dihydroxyvitamin D3-responsive epithelia. *J. Biol. Chem.* **274,** 8375–8378
11. Woudenberg-Vrenken, T. E., Bindels, R. J., and Hoenderop, J. G. (2009) The role of transient receptor potential channels in kidney disease. *Nat. Rev. Nephrol.* **5,** 441–449
12. Pansu, D., Duflos, C., Bellaton, C., and Bronner, F. (1993) Solubility and intestinal transit time limit calcium absorption in rats. *J. Nutr.* **123,** 1396–1404
13. Perez, A. V., Picotto, G., Carpentieri, A. R., Rivoira, M. A., Peralta Lopez, M. E., and Tolosa de Talamoni, N. G. (2008) Minireview on regulation of intestinal calcium absorption. Emphasis on molecular mechanisms of transcellular pathway. *Digestion* **77,** 22–34
14. Flik, G., Verbost, P. M., and Wendelaar Bongar, S. E. (1995) Calcium transport process in fishes. In *Cellular and Molecular Approaches to Fish Ionic Regulation* (Wood, C. M., and Shuttleworth, T. J., eds) pp. 317–342, Academic Press, San Diego, CA, USA
15. Ishihara, A., and Mugiya, Y. (1987) Ultrastructural evidence of calcium uptake by chloride cells in the gills of goldfish, *Carassius auratus*. *J. Exp. Zoology* **242,** 121–129
16. Liao, B. K., Deng, A. N., Chen, S. C., Chou, M. Y., and Hwang, P. P. (2007) Expression and water calcium dependence of calcium transporter isoforms in zebrafish gill mitochondrion-rich cells. *BMC Genomics* **8,** 354
17. Vennekens, R., Owsianik, G., and Nilius, B. (2008) Vanilloid transient receptor potential cation channels: an overview. *Curr. Pharm. Des.* **14,** 18–31
18. Benham, C. D., Davis, J. B., and Randall, A. D. (2002) Vanilloid and TRP channels: a family of lipid-gated cation channels. *Neuropharmacology* **42,** 873–888
19. Nilius, B., Weidema, F., Prenen, J., Hoenderop, J. G., Vennekens, R., Hoefs, S., Droogmans, G., and Bindels, R. J. (2003) The carboxyl terminus of the epithelial Ca(2+) channel ECaC1 is involved in Ca(2+)-dependent inactivation. *Pflügers Arch.* **445,** 584–588
20. Nilius, B., Vennekens, R., Prenen, J., Hoenderop, J. G., Bindels, R. J., and Droogmans, G. (2000) Whole-cell and single channel monovalent cation currents through the novel rabbit epithelial Ca^{2+} channel ECaC. *J. Physiol.* **527,** 239–248
21. Nilius, B., Vennekens, R., Prenen, J., Hoenderop, J. G., Droogmans, G., and Bindels, R. J. (2001) The single pore residue Asp542 determines Ca^{2+} permeation and Mg^{2+} block of the epithelial Ca^{2+} channel. *J. Biol. Chem.* **276,** 1020–1025
22. Vennekens, R., Hoenderop, J. G., Prenen, J., Stuiver, M., Willems, P. H., Droogmans, G., Nilius, B., and Bindels, R. J. (2000) Permeation and gating properties of the novel epithelial Ca(2+) channel. *J. Biol. Chem.* **275,** 3963–3969
23. Bronner, F. (2009) Recent developments in intestinal calcium absorption. *Nutr. Rev.* **67,** 109–113

24. Bronner, F., Slepchenko, B., Wood, R. J., and Pansu, D. (2003) The role of passive transport in calcium absorption. *J. Nutr.* **133,** 1426; author reply 1427
25. Bianco, S. D., Peng, J. B., Takanaga, H., Suzuki, Y., Crescenzi, A., Kos, C. H., Zhuang, L., Freeman, M. R., Gouveia, C. H., Wu, J., Luo, H., Mauro, T., Brown, E. M., and Hediger, M. A. (2007) Marked disturbance of calcium homeostasis in mice with targeted disruption of the Trpv6 calcium channel gene. *J. Bone Miner. Res.* **22,** 274–285
26. Hoenderop, J. G., van Leeuwen, J. P., van der Eerden, B. C., Kersten, F. F., van der Kemp, A. W., Merillat, A. M., Waarsing, J. H., Rossier, B. C., Vallon, V., Hummler, E., and Bindels, R. J. (2003) Renal Ca^{2+} wasting, hyperabsorption, and reduced bone thickness in mice lacking TRPV5. *J. Clin. Invest.* **112,** 1906–1914
27. Datta, H. K., Ng, W. F., Walker, J. A., Tuck, S. P., and Varanasi, S. S. (2008) The cell biology of bone metabolism. *J. Clin. Pathol.* **61,** 577–587
28. Renn, J., Winkler, C., Schartl, M., Fischer, R., and Goerlich, R. (2006) Zebrafish and medaka as models for bone research including implications regarding space-related issues. *Protoplasma* **229,** 209–214
29. Spoorendonk, K. M., Hammond, C. L., Huitema, L. F. A., Vanoevelen, J., and Schulte-Merker, S. (2010) Zebrafish as a unique model system in bone research: the power of genetics and in vivo imaging. *J. Appl. Ichtyology* **26,** 219–224
30. Walker, M. B., and Kimmel, C. B. (2007) A two-color acid-free cartilage and bone stain for zebrafish larvae. *Biotech Histochem.* **82,** 23–28
31. Schulte-Merker, S. (2002) Looking at embryos. In *Zebrafish: A Practical Approach* (Nusslein-Volhard, C., and Dahm, R., eds) pp. 39–58, Oxford University Press, New York
32. Hammond, C. L., and Schulte-Merker, S. (2009) Two populations of endochondral osteoblasts with differential sensitivity to Hedgehog signalling. *Development* **136,** 3991–4000
33. Greenwood, M. P., Flik, G., Wagner, G. F., and Balment, R. J. (2009) The corpuscles of Stannius, calcium-sensing receptor, and stanniocalcin: responses to calcimimetics and physiological challenges. *Endocrinology* **150,** 3002–3010
34. Renn, J., and Winkler, C. (2009) Osterix-mCherry transgenic medaka for in vivo imaging of bone formation. *Dev. Dyn.* **238,** 241–248
35. Kawakami, K., Koga, A., Hori, H., and Shima, A. (1998) Excision of the tol2 transposable element of the medaka fish, *Oryzias latipes*, in zebrafish, *Danio rerio. Gene* **225,** 17–22
36. Inohaya, K., Takano, Y., and Kudo, A. (2007) The teleost intervertebral region acts as a growth center of the centrum: in vivo visualization of osteoblasts and their progenitors in transgenic fish. *Dev. Dyn.* **236,** 3031–3046
37. Brand, M., Granato, M., and Nusslein-Volhard, C. (2002) Keeping and raising zebrafish. In *Zebrafish: A Practical Approach* (Nusslein-Volhard, C., and Dahm, R., eds) pp. 7–37, Oxford University Press, New York
38. Shahsavarani, A., McNeill, B., Galvez, F., Wood, C. M., Goss, G. G., Hwang, P. P., and Perry, S. F. (2006) Characterization of a branchial epithelial calcium channel (ECaC) in freshwater rainbow trout (*Oncorhynchus mykiss*). *J. Exp. Biol.* **209,** 1928–1943
39. Lafeber, F. P., Hanssen, R. G., Choy, Y. M., Flik, G., Herrmann-Erlee, M. P., Pang, P. K., and Bonga, S. E. (1988) Identification of hypocalcin (teleocalcin) isolated from trout Stannius corpuscles. *Gen. Comp. Endocrinol.* **69,** 19–30
40. Tseng, D. Y., Chou, M. Y., Tseng, Y. C., Hsiao, C. D., Huang, C. J., Kaneko, T., and Hwang, P. P. (2009) Effects of stanniocalcin 1 on calcium uptake in zebrafish (*Danio rerio*) embryo. *Am. J. Physiol. Regul. Integr. Comp. Physiol.* **296,** R549–R557
41. Pang, P. K., and Pang, R. K. (1974) Environmental calcium and hypocalcin activity in the Stannius corpuscles of the channel catfish, *Ictalurus punctatus* (Rafinesque). *Gen. Comp. Endocrinol.* **23,** 239–241
42. Peltz, S. W., Brown, A. H., and Jacobson, A. (1993) mRNA destabilization triggered by premature translational termination depends on at least three cis-acting sequence elements and one trans-acting factor. *Genes Dev.* **7,** 1737–1754
43. Chen, Y. Y., Lu, F. I., and Hwang, P. P. (2003) Comparisons of calcium regulation in fish larvae. *J. Exp. Zool. A Comp. Exp. Biol.* **295,** 127–135
44. Chou, M. Y., Yang, C. H., Lu, F. I., Lin, H. C., and Hwang, P. P. (2002) Modulation of calcium balance in tilapia larvae (*Oreochromis mossambicus*) acclimated to low-calcium environments. *J. Comp. Physiol. B* **172,** 109–114
45. Elizondo, M. R., Arduini, B. L., Paulsen, J., MacDonald, E. L., Sabel, J. L., Henion, P. D., Cornell, R. A., and Parichy, D. M. (2005) Defective skeletogenesis with kidney stone formation in dwarf zebrafish mutant for trpm7. *Curr. Biol.* **15,** 667–671
46. Elizondo, M. R., Budi, E. H., and Parichy, D. M. (2010) Trpm7 regulation of in vivo cation homeostasis and kidney function involves stanniocalcin 1 and fgf23. *Endocrinology* **151,** 5700–5709
47. Krakow, D., Vriens, J., Camacho, N., Luong, P., Deixler, H., Funari, T. L., Bacino, C. A., Irons, M. B., Holm, I. A., Sadler, L., Okenfuss, E. B., Janssens, A., Voets, T., Rimoin, D. L., Lachman, R. S., Nilius, B., and Cohn, D. H. (2009) Mutations in the gene encoding the calcium-permeable ion channel TRPV4 produce spondylometaphyseal dysplasia, Kozlowski type and metatropic dysplasia. *Am. J. Hum. Genet.* **84,** 307–315
48. Rock, M. J., Prenen, J., Funari, V. A., Funari, T. L., Merriman, B., Nelson, S. F., Lachman, R. S., Wilcox, W. R., Reyno, S., Quadrelli, R., Vaglio, A., Owsianik, G., Janssens, A., Voets, T., Ikegawa, S., Nagai, T., Rimoin, D. L., Nilius, B., and Cohn, D. H. (2008) Gain-of-function mutations in TRPV4 cause autosomal dominant brachyolmia. *Nat. Genet.* **40,** 999–1003
49. Deng, H. X., Klein, C. J., Yan, J., Shi, Y., Wu, Y., Fecto, F., Yau, H. J., Yang, Y., Zhai, H., Siddique, N., Hedley-Whyte, E. T., Delong, R., Martina, M., Dyck, P. J., and Siddique, T. (2010) Scapuloperoneal spinal muscular atrophy and CMT2C are allelic disorders caused by alterations in TRPV4. *Nat. Genet.* **42,** 165–169
50. Landoure, G., Zdebik, A. A., Martinez, T. L., Burnett, B. G., Stanescu, H. C., Inada, H., Shi, Y., Taye, A. A., Kong, L., Munns, C. H., Choo, S. S., Phelps, C. B., Paudel, R., Houlden, H., Ludlow, C. L., Caterina, M. J., Gaudet, R., Kleta, R., Fischbeck, K. H., and Sumner, C. J. (2010) Mutations in TRPV4 cause Charcot-Marie-Tooth disease type 2C. *Nat. Genet.* **42,** 170–174
51. Hoenderop, J. G., Vennekens, R., Muller, D., Prenen, J., Droogmans, G., Bindels, R. J., and Nilius, B. (2001) Function and expression of the epithelial Ca(2+) channel family: comparison of mammalian ECaC1 and 2. *J. Physiol.* **537,** 747–761
52. Qiu, A., and Hogstrand, C. (2004) Functional characterisation and genomic analysis of an epithelial calcium channel (ECaC) from pufferfish, *Fugu rubripes. Gene* **342,** 113–123
53. Van der Eerden, B. C., Hoenderop, J. G., de Vries, T. J., Schoenmaker, T., Buurman, C. J., Uitterlinden, A. G., Pols, H. A., Bindels, R. J., and van Leeuwen, J. P. (2005) The epithelial Ca^{2+} channel TRPV5 is essential for proper osteoclastic bone resorption. *Proc. Natl. Acad. Sci. U. S. A.* **102,** 17507–17512
54. Suzuki, Y., Kovacs, C. S., Takanaga, H., Peng, J. B., Landowski, C. P., and Hediger, M. A. (2008) Calcium channel TRPV6 is involved in murine maternal-fetal calcium transport. *J. Bone Miner. Res.* **23,** 1249–1256
55. Benn, B. S., Ajibade, D., Porta, A., Dhawan, P., Hediger, M., Peng, J. B., Jiang, Y., Oh, G. T., Jeung, E. B., Lieben, L., Bouillon, R., Carmeliet, G., and Christakos, S. (2008) Active intestinal calcium transport in the absence of transient receptor potential vanilloid type 6 and calbindin-D9k. *Endocrinology* **149,** 3196–3205
56. Lieben, L., Benn, B. S., Ajibade, D., Stockmans, I., Moermans, K., Hediger, M. A., Peng, J. B., Christakos, S., Bouillon, R., and Carmeliet, G. (2010) Trpv6 mediates intestinal calcium absorption during calcium restriction and contributes to bone homeostasis. *Bone* **47,** 301–308
57. Kutuzova, G. D., Sundersingh, F., Vaughan, J., Tadi, B. P., Ansay, S. E., Christakos, S., and Deluca, H. F. (2008) TRPV6 is not required for 1alpha,25-dihydroxyvitamin D3-induced intestinal calcium absorption in vivo. *Proc. Natl. Acad. Sci. U. S. A.* **105,** 19655–19659
58. Koushik, S. V., Wang, J., Rogers, R., Moskophidis, D., Lambert, N. A., Creazzo, T. L., and Conway, S. J. (2001) Targeted inactivation of the sodium-calcium exchanger (Ncx1) results in the lack of a heartbeat and abnormal myofibrillar organization. *FASEB J.* **15,** 1209–1211
59. Okunade, G. W., Miller, M. L., Pyne, G. J., Sutliff, R. L., O'Connor, K. T., Neumann, J. C., Andringa, A., Miller, D. A., Prasad, V., Doetschman, T., Paul, R. J., and Shull, G. E. (2004) Targeted ablation of plasma membrane Ca^{2+}-ATPase (PMCA) 1 and 4 indicates a major housekeeping function for PMCA1 and a critical role in hyperactivated sperm motility and male fertility for PMCA4. *J. Biol. Chem.* **279,** 33742–33750

Received for publication February 11, 2011.
Accepted for publication June 2, 2011.